Inorg. Chem. **2006**, *45*, 10951–10957

Spectroscopic and Ab Initio Characterization of the $[ReH_9]^{2-}$ Ion

Stewart F. Parker,*,† Keith Refson,‡ Kenneth P. J. Williams,§ Dale A. Braden,#,⊥ Bruce S. Hudson,|| and Klaus Yvon£

ISIS Facility, Rutherford Appleton Laboratory, Chilton, Didcot, Oxfordshire OX11 0QX, U.K., Computational Materials Science Group, Rutherford Appleton Laboratory, Chilton, Didcot, Oxfordshire OX11 0QX, U.K., Transducer System Division, Renishaw plc, Old Town, Wotton-under-Edge, Gloucestershire GL12 7DL, U.K., Department of Chemistry, University of Oregon, Eugene, Oregon 97403-1253, Department of Chemistry, Syracuse University, Syracuse, New York 13244-4100, and Laboratoire de Cristallographie, Universite de Geneve, 24 quai Ernest Ansermet, CH 1211 Geneve 4, Switzerland

Received June 29, 2006

The dynamics and bonding of the hydrido complex $Ba[ReH_9]$, containing the D_{3h} face-capped trigonal prismatic $[ReH_9]^{2-}$ ion, have been investigated by vibrational spectroscopy and density functional theory (DFT). The combination of infrared, Raman, and inelastic neutron-scattering (INS) spectroscopies has enabled observation of all the modes of the $[ReH_9]^{2-}$ ion for the first time. We demonstrate that calculations of the isolated $[ReH_9]^{2-}$ ion are unable to reproduce the INS spectrum and that the complete unit cell must be considered with periodic DFT to have reliable results. This is shown to be a consequence of the long-range Coulomb potential present. Analysis of the electronic structure shows that the bonding between the rhenium and the hydrogen is largely covalent. There is a small degree of covalency between the prism hydrides and the barium. The counterion is crucial to the stability of the materials; hence, variation of it potentially offers a method to fine-tune the properties of the material.

Introduction

In recent years, a wide variety of hydride complexes of the form $A_x[MH_y]$ (A = alkali or alkaline earth metal, M = transition metal) have been synthesized.[1] However, one of the very first to be obtained,[2] the $[ReH_9]^{2-}$ ion, continues to occupy a central place in chemistry. This is because of the unusually high formal oxidation state of the metal, +VII, its high symmetry,[3] D_{3h}, a face-capped trigonal prism (see Figure 1), and its stability. The complex has an extensive organometallic chemistry with many derivatives of the type $[ReH_{9-x}(PR_3)_x]^{2-}$ ($x = 2-5$) known.[4] In solution, some of these have been shown to have both hydrido and dihydrogen ligands (e.g., $[ReH_6(\eta^2\text{-}H_2)(dppen)]^+$, dppen = *cis*-1,2-bis-(diphenylphosphino)ethylene.[5] The parent ion is also of considerable interest as a model system for hydrogen storage applications since the barium salt,[6] $Ba[ReH_9]$, has the highest known hydrogen-to-metal ratio, 4.5:1. However, the hydrogen content is only 1.3 wt % which is well below the DOE target of 6 wt % so it is not a viable hydrogen-storage material.

The bonding in ternary metal hydrides has been extensively investigated by theoretical methods,[7−10] although the

* To whom correspondence should be addressed. E-mail: s.f.parker@rl.ac.uk.
† ISIS Facility.
‡ Computational Materials Science Group.
§ Renishaw plc.
# University of Oregon.
|| Syracuse University.
£ Universite de Geneve.
⊥ Present address: Schrodinger, Inc., 101 SW Main St., Suite 1300, Portland, Oregon 97204.

(1) Yvon, K.; Renaudin, G. In *Encyclopedia of Inorganic Chemistry*, 2nd ed.; King, R. B., Ed.; John Wiley: New York, 2005; pp 1814−1846.
(2) Ginsberg, A. P.; Miller, J. M.; Koubek, E. *J. Am. Chem. Soc.* **1961**, *83*, 4909.
(3) Abrahams, S. C.; Ginsberg, A. P.; Knox, K. *Inorg. Chem.* **1964**, *3*, 558.
(4) Cotton, F. A.; Wilkinson, G.; Murillo, C. A.; Bochmann, M. *Advanced Inorganic Chemistry*, 6th ed.; John Wiley: New York, 1999; Chapter 18-D-10, p 995.
(5) Fontaine, X. L. R.; Layzell, T. P.; Shaw, B. L. *J. Chem. Soc., Dalton Trans.* **1994**, 917.
(6) Stetson, N. T.; Yvon, K.; Fischer, P. *Inorg. Chem.* **1994**, *33*, 4598.
(7) Olofsson-Mårtensson, M.; Häussermann, U.; Tomkinson, J.; Noréus, D. *J. Am. Chem. Soc.* **2000**, *122*, 6960−6970.
(8) Parker, S. F.; Bennington, S. M.; Ramirez-Cuesta, A. J.; Auffermann, G.; Bronger, W.; Herman, H.; Williams, K. P. J.; Smith, T. *J. Am. Chem. Soc.* **2003**, *125*, 11656−11661.
(9) King, R. B. *Coord. Chem. Rev.* **2000**, *200*−*202*, 813−829.
(10) Maseras, F.; Lledos, A.; Clot, E.; Eisenstein, O. *Chem. Rev.* **2000**, *100*, 601−636.

10.1021/ic0611894 CCC: $33.50
Published on Web 12/01/2006

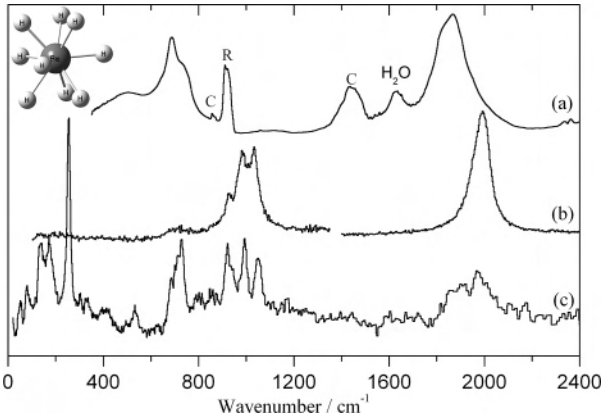

Figure 1. (a) Infrared, (b) Raman, and (c) INS spectra of $Ba[ReH_9]$. In spectrum a, decomposition products are marked as C (carbonate) and R (rhenate). The peak at 1610 cm^{-1} is from the water in the KBr disk. In spectrum b, the range of 100−1350 cm^{-1} is 2.5 times ordinate-expanded relative to 1400−2400 cm^{-1}. The structure of the $[ReH_9]^{2-}$ ion is shown at the top left.

particular case of the $[ReH_9]^{2-}$ ion is represented by only one ab initio investigation of the isolated ion[11] and one periodic calculation of the complete unit cell.[12]

The vibrational spectrum of the ion has been investigated a number of times by infrared and Raman spectroscopies;[13,14] however, the high symmetry results in two inactive modes. In addition, as has been found recently for other metal hydride complexes,[15] even when the modes are infrared or Raman allowed, they may still be too weak to be observed. In principle, inelastic neutron-scattering (INS) spectroscopy[16] is the ideal technique to study these materials since all of the modes are allowed; however, the only previous INS study[17] was restricted to a small energy-transfer range and was of modest resolution.

In this paper, we have investigated the $[ReH_9]^{2-}$ ion, both as an isolated ion and as the barium salt,[6] at different levels of theory. We have obtained the first complete vibrational spectrum of the $[ReH_9]^{2-}$ ion and used it to validate the ab initio results by comparison of the observed and calculated INS and infrared spectra. Having established the reliability of the results, we then used the ab initio results to describe the bonding in $Ba[ReH_9]$.

Experimental Section

$Ba[ReH_9]$. $Ba[ReH_9]$ was prepared in Switzerland by metathesis of the disodium salt as described previously.[6] The compound was characterized by X-ray diffraction and shown to be of high purity. It was transported to the U.K. in a glass ampule sealed under argon.

Vibrational Spectroscopy. Mid-infrared, 4000−400 cm^{-1}, spectra were recorded at room temperature from KBr discs with a Digilab FTS-60 Fourier transform infrared spectrometer equipped with a room-temperature deuterated triglycine sulfate detector using 256 scans at 4 cm^{-1} resolution with triangular apodization. The compound is somewhat air sensitive, and the necessity of preparing the KBr discs in air resulted in some decomposition. Raman spectra were recorded using a Renishaw 2000 dispersive Raman microscope spectrometer with 514.5 nm excitation from an argon ion laser. The spectra were recorded from the sample in the glass ampule. Both the infrared and Raman spectra were recorded at room temperature. The INS experiments were performed using the high-resolution broadband spectrometer, TFXA,[16] at the ISIS pulsed spallation neutron source at the Rutherford Appleton Laboratory, Chilton, U.K. TFXA offered high resolution, ∼2% of the energy transfer between 16 and 4000 cm^{-1}. INS spectroscopy is sensitive to all wavevectors; thus the trajectory that the spectrometer takes through the neighboring Brillouin zones of the sample means that each zone is sampled differently. Since the dynamics of every zone is replicated in that of the first zone the result is that a good sampling of the Brillouin zone is obtained.[16] For these measurements, the compound was loaded into an indium wire-sealed aluminum can in an argon glovebox. The sample was then cooled to 20 K, and the spectrum recorded. The INS spectrum is available from the INS database[18] at www.isis.rl.ac.uk/insdatabase.

Ab Initio Studies. Solid $Ba[ReH_9]$ was investigated with periodic DFT using a plane-wave basis set and pseudopotentials as implemented in the CASTEP code.[19−21] The PBE[22] version of the generalized gradient approximation within DFT was used in conjunction with optimized norm-conserving pseudopotentials generated using the Qc-tuning method.[23,24] The Brillouin zone (BZ) sampling used a 5 × 5 × 4 grid of k-points in the full BZ, generated using the Monkhorst-Pack method,[25] which converged the total energy to 40 μeV/atom and forces to better than 0.1 meV/Å. A plane-wave cutoff energy of 440 eV gave an energy convergence of 10 meV/atom, a force convergence of 5 meV/Å, and frequency convergence better than 11 cm^{-1} (tested on an isolated ion calculation). Phonon modes were calculated using density-functional perturbation theory[21,26] to compute the dynamical matrices on a grid of phonon wavevectors which were Fourier interpolated to generate full dispersion curves.[27,28] As a prerequisite to any lattice dynamics calculation, a full geometry optimization of the internal atomic coordinates was performed to reduce the residual atomic forces to better than 1.5 meV/Å.

The isolated ion was investigated with density functional theory (DFT) both with CASTEP as with the crystalline-state calculations and with a range of basis sets and functionals as implemented in

(11) Shen, M.; Schaefer, H. F., III; Partridge. H. *Mol. Phys.* **1992**, *76*, 995−1007.
(12) Orgaz, E.; Gupta, M. *J. Alloys Cmpds.* **1999**, *293*−*295*, 217−221.
(13) Ginsberg, A. P.; Sprinkle, C. R. *Inorg. Chem.* **1969**, *8*, 2212.
(14) Creighton, J. A.; Sinclair, T. J. *J. Chem. Soc., Faraday Trans. II* **1974**, *70*, 548.
(15) Parker, S. F.; Williams, K. P. J.; Bortz, M. Yvon, K. *Inorg. Chem.* **1997**, *36*, 5218.
(16) Mitchell, P. C. H.; Parker, S. F.; Ramirez-Cuesta, A. J.; Tomkinson, J. *Vibrational Spectroscopy with Neutrons, with Applications in Chemistry, Biology, Materials Science and Catalysis*; World Scientific: Singapore, 2005.
(17) White, J. W.; Wright, C. J. *J. Chem. Soc., Faraday Trans. II* **1972**, *68*, 1414.
(18) Parker, S. F.; Champion, D. J. *Internet J. Vib. Spec.* **1999**, *3* (3), http://www.ijvs.com/volume3/edition3/section1.html#Feature.
(19) Segall, M. D.; Lindan, P. J. D.; Probert, M. J.; Pickard, C. J.; Hasnip, P. J.; Clark, S. J.; Payne, M.C. *J. Phys.: Condens. Mat.* **2002**, *14*, 2717.
(20) Clark, S. J.; Segall, M. D.; Pickard, C. J.; Hasnip, P. J.; Probert, M. J.; Refson, K.; Payne, M.C. *Z. Kristallogr.* **2005**, *220*, 567.
(21) Refson, K.; Tulip, P. R.; Clark, S. J. *Phys. Rev. B* **2006**, 73, 155114.
(22) Perdew, J. P; Burke, K.; Enzerhof, M. *Phys. Rev. Lett.* **1996**, *77*, 3865.
(23) Lin, J.S.; Qteish A.; Payne, M. C.; Heine, V. *Phys Rev B* **1993**, *47*, 4714.
(24) Lee, M. H. Ph.D. Thesis, Cambridge University, Cambridge, U.K., 1995. http://psi-k.dl.ac.uk/newsletters/News_67/Highlight_67.pdf.
(25) Monkhorst, H. J.; Pack, J. D. *Phys. Rev. B* **1976**, *13*, 5188.
(26) Gonze, X. *Phys. Rev. B* **1997**, *55*, 10377.
(27) Giannozzi, P.; de Gironcoli, S.; Pavone, P.; Baroni, S. *Phys. Rev. B* **1991**, *43*, 7231.
(28) Gonze, X.; Lee, C. *Phys. Rev. B* **1977**, *55*, 10355.

Table 1. Comparison of Ab Initio Calculations for the Isolated $[ReH_9]^{2-}$ Ion with a Range of Methods and Basis Sets[a]

bond length/Å	SSP I[b]	SSP III[b]	QCISD sdd60 mwb/ tzv+p	BP86 aug-cc-pVTZ/ std grid	BP86/ cc-pVTZ/ ultrafine grid	mPW-PW aug-cc-pVTZ / ultrafine grid	B3LYP tzv+p/ ultrafine grid	B3LYP tzv+p/ sdd-4d	B3LYP tzv+p/ sdd(2f,1d)	B3LYP tzv+2p/ sdd+	B3LYP cc-pvqz/ sdd+	PBE CASTEP (440 eV)
						bond length (Å)						
$Re-H_{cap}$	1.689	1.687	1.669	1.699	1.699	1.698	1.691	1.691	1.692	1.692	1.700	1.689
$Re-H_{prism}$	1.741	1.742	1.711	1.736	1.735	1.734	1.729	1.729	1.730	1.731	1.736	1.718
						symmetry[c] and activity[d] (cm^{-1})						
E'(R, IR)	365	355	312	303	309	309	331	332	331	328	328	307
E'(R, IR)	693	614	677	642	647	642	685	685	676	670	670	645
A_2''(IR)	673	608	720	656	660	656	696	694	690	683	690	671
A_1''(ia)	748	724	755	713	722	717	759	761	759	759	756	711
E''(R)	819	812	812	740	746	742	786	787	785	782	785	735
A_2''(IR)	980	916	839	794	801	795	860	860	851	840	844	783
A_2'(ia)	1009	930	813	828	835	829	895	896	888	880	878	817
A_1'(R)	1009	985	1007	881	885	884	940	939	937	928	924	889
E' (R, IR)	1023	977	933	903	911	908	969	970	966	959	952	908
E''(R)	1056	993	959	922	924	920	986	986	982	978	972	922
A_2''(IR)	1733	1719	1796	1679	1693	1685	1725	1718	1710	1705	1701	1701
E'(R, IR)	1711	1702	1810	1692	1708	1701	1737	1729	1722	1717	1712	1717
E''(R)	1743	1735	1843	1740	1755	1748	1783	1777	1769	1764	1757	1768
A_1'(R)	1792	1797	1915	1787	1798	1793	1830	1823	1817	1814	1806	1819
E'(R, IR)	1932	1940	2000	1865	1872	1867	1912	1906	1900	1899	1893	1897
A_1'(R)	2013	2022	2038	1921	1928	1925	1978	1976	1972	1970	1965	1946

[a] All calculations were performed with GAUSSIAN98 except those in the last column which used CASTEP. [b] Ref 11, Hartree−Fock based methods, SSP III used a larger basis set than SSP I. [c] Symmetry labels are for D_{3h} symmetry. [d] Activity: IR = infrared allowed, R = Raman allowed, ia = inactive in both Raman and infrared. Note all modes are INS allowed.

GAUSSIAN98.[29] The details are given in Table 1. To compute the frequencies using periodic boundary conditions as implemented in CASTEP, it was necessary to perform calculations of a molecular ion surrounded by vacuum at a number of periodic box sizes and extrapolate to infinite ion separation.

The INS spectra were generated from the ab initio output using the program ACLIMAX[30] (available from www.isis.rl.ac.uk/molecularspectroscopy).

Results and Discussion

Structure. The face-capped trigonal prismatic D_{3h} structure of the $[ReH_9]^{2-}$ ion has two types of Re−H bond; the latest neutron diffraction determination[31] (as the dipotassium salt) gives 1.677 and 1.689 Å for the face-capping ($Re-H_{cap}$) and trigonal prismatic ($Re-H_{prism}$) Re−H distances, respectively. The isolated-ion DFT calculations slightly overestimate these as is usual in the GGA approximation, with distances in the range of $Re-H_{cap}$ = 1.669−1.700 Å and $Re-H_{prism}$ = 1.71−1.736 Å (Table 1). Hartree−Fock calculations[11] with very large basis sets gave $Re-H_{cap}$ = 1.686 Å and $Re-H_{prism}$ = 1.742 Å.

For the periodic DFT CASTEP calculations, the structure was energy minimized (geometry optimization but not lattice optimization) starting from the experimental crystal structure.[6] This converged to a stable D_{3h} structure (literature $Re-H_{cap} = Re-H_{prism}$ = 1.69 Å; ab initio $Re-H_{cap}$ = 1.668 Å, $Re-H_{prism}$ = 1.705 Å). In the original structure determination, the hydrides were not located but were assigned to assumed positions on the basis of a reasonable geometry.[6] The present work confirms the face-capped trigonal prismatic D_{3h} structure of the $[ReH_9]^{2-}$ ion in $Ba[ReH_9]$, and there are no indications of any Re−H−Re bonding. We note that the shortest intramolecular H−H distance is 1.915 Å: this is considerably greater than the longest known H−H distance in a dihydrogen complex of ∼1.3 Å.[32] Thus the calculations are fully consistent with the formulation of the $[ReH_9]^{2-}$ ion as a mononuclear homoleptic hydride rather than a hydride−dihydrogen complex.

Vibrational Spectroscopy. The vibrational spectra of $Ba[ReH_9]$ are shown in Figure 1. In agreement with previous work,[6] the infrared spectrum, Figure 1a, has a strong band at 1870 cm^{-1} with a shoulder at 1830 cm^{-1} and a second strong band at 684 cm^{-1} with shoulders at 740 and 634 cm^{-1}. Decomposition products are apparent at 917 (rhenate, R), 861, and 1434 cm^{-1} (carbonate, C). The Raman spectrum, Figure 1b, which has not been observed before, has an intense, somewhat asymmetric band at 1992 cm^{-1} and weaker features at 1034, 983, 925, and 711 cm^{-1}. The INS spectrum, Figure 1c, shows bands across the entire range, 2400−20 cm^{-1}.

There are no selection rules for the INS spectrum, and all modes are allowed.[16] The INS intensities depend on the

(29) Frisch, M. J.; Trucks, G. W.; Schlegel, H. B.; Scuseria, G. E.; Robb, M. A.; Cheeseman, J. R.; Zakrzewski, V. G.; Montgomery, J. A., Jr.; Stratmann, R. E.; Burant, J. C.; Dapprich, S.; Millam, J. M.; Daniels, A. D.; Kudin, K. N.; Strain, M. C.; Farkas, O.; Tomasi, J.; Barone, V.; Cossi, M.; Cammi, R.; Mennucci, B.; Pomelli, C.; Adamo, C.; Clifford, S.; Ochterski, J.; Petersson, G. A.; Ayala, P. Y.; Cui, Q.; Morokuma, K.; Malick, D. K.; Rabuck, A. D.; Raghavachari, K.; Foresman, J. B.; Cioslowski, J.; Ortiz, J. V.; Stefanov, B. B.; Liu, G.; Liashenko, A.; Piskorz, P.; Komaromi, I.; Gomperts, R.; Martin, R. L.; Fox, D. J.; Keith, T.; Al-Laham, M. A.; Peng, C. Y.; Nanayakkara, A.; Gonzalez, C.; Challacombe, M.; Gill, P. M. W.; Johnson, B. G.; Chen, W.; Wong, M. W.; Andres, J. L.; Head-Gordon, M.; Replogle, E. S.; Pople, J. A. *Gaussian98*, revision A.6; Gaussian Inc.: Pittsburgh, PA, 1998.
(30) Ramirez-Cuesta, A. J. *Comput. Phys. Commun.* **2004,** *157*, 226−238.
(31) Bronger, W.; á Brassard, L.; Miller, P.; LeBech, B.; Schultz, Th. *Z. Anorg. Allg. Chem.* **1999**, *625*, 1143−1146.
(32) Kubas, G. J. *Metal Dihydrogen and σ-Bond Complexes*; Kluwer Academic: New York, 2001; p 82.

incoherent cross-section and the amplitude of vibration of the atoms. The large incoherent cross-section and the light mass of hydrogen means that modes that involve motion of hydrogen will dominate the INS spectrum. In the present case, all of the internal modes and the librational modes would be expected to appear strongly in INS spectrum, the translational modes of the $[ReH_9]^{2-}$ ion will appear weakly, and the translational modes of the Ba^{2+} ion will be very weak or absent.

$Ba[ReH_9]$ contains two formula units in the unit cell,[6] and both $[ReH_9]^{2-}$ ions occupy D_{3h} sites. From the spectra, the factor-group splitting is small, so initially, we can treat the spectrum as being that of an isolated $[ReH_9]^{2-}$ ion. (We will include the factor-group splitting later.) An isolated D_{3h} $[ReH_9]^{2-}$ ion has 24 vibrations, which are distributed as 16 modes: 9 Re−H stretches, $2A_1'(R) + 2E'(IR, R) + A_2''(IR) + E''(R)$, and 15 H−Re−H bends, $A_1'(R) + A_2'(ia) + 3E'(IR, R) + A_1''(ia) + 2A_2''(IR) + 2E''(R)$ (IR = infrared active, R = Raman active, ia = inactive in both infrared and Raman).

It is clear that many fewer modes are observed in the infrared and Raman spectra than expected, and this is the major problem encountered by previous workers.[12,13] Surprisingly, the INS spectrum does not show clear evidence for the missing modes: three modes are apparent in the stretching region, while below 1100 cm^{-1}, three are clearly visible between 800 and 1100 cm^{-1}; there is a complex feature near 700 cm^{-1}, and there are three intense bands at 130, 170, and 250 cm^{-1}. Curve fitting the complex 700 cm^{-1} feature indicates three bands at 680, 705, and 730 cm^{-1} in good agreement with the observed infrared and Raman bands. The intense feature at 256 cm^{-1} is also assigned as an internal mode. Thus a maximum of eight bands in the bending region and three in the stretching region are apparent. Since *all* of the internal modes *must* be present in the INS spectrum with comparable intensities (*E* modes being approximately twice as intense as *A* modes), this means that the "missing" modes are accidentally degenerate (or at least separated by less than the instrumental resolution) with the "observed" modes.

To assign the vibrational spectra, we have carried out ab initio density functional theory calculations of both the isolated ion and the complete unit cell. From Table 1, for the isolated ion, it can be seen that the frequencies vary by up to 50 cm^{-1} depending on the choice of method, functional, and basis set. INS intensities only depend on the incoherent scattering cross-section and the amplitude of vibration.[16] The latter is available from the ab initio output and the INS spectrum is then calculated by ACLIMAX.[27]An example of an isolated-ion calculation is shown in Figure 2d.

For the complete unit cell, we have carried out periodic DFT calculations using CASTEP at both the Γ-point to obtain symmetry labels and infrared intensities and also across the complete Brillouin zone, including longitudinal optic−transverse optic (LOTO) splitting. Figure 2b and c shows the results for the complete Brillouin zone. It can be seen that the agreement is generally good, and this is particularly the case for the internal modes of the $[ReH_9]^{2-}$ ion. We note that the shape of the band at 925 cm^{-1} is well-produced.

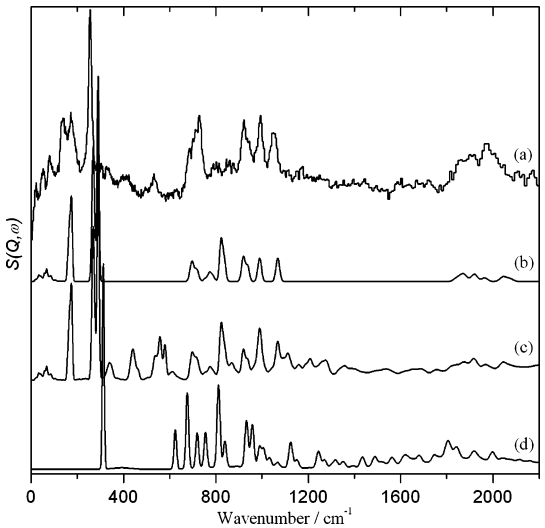

Figure 2. Comparison of INS spectra of $Ba[ReH_9]$: (a) experimental and (b) calculated with CASTEP for the complete unit cell across the entire Brillouin zone (one phonon contribution only). Spectrum c is the same as b but up to and including 10 phonon events, and spectrum d was calculated with GAUSSIAN98 for an isolated $[ReH_9]^{2-}$ ion using QCISD sdd60mwb/tzv+p.

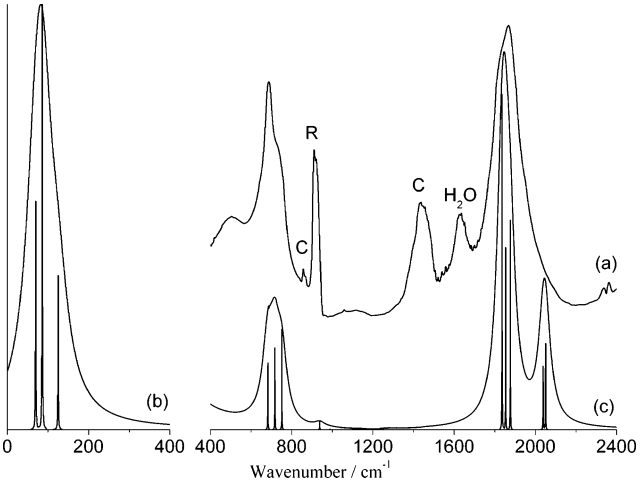

Figure 3. Comparison of (a) observed and (b, c) calculated infrared spectra of $Ba[ReH_9]$. Spectrum c is 5 times ordinate-expanded relative to spectrum b.

The only mode that is miscalculated is that at 823 cm^{-1} (observed at 731 cm^{-1}), and the error is only 12%; all the other internal modes are calculated with an error of less than 5%. Inclusion of LOTO splitting alters four E_{1u} modes: one translation, one bending, and two stretching modes. We have also calculated the infrared intensities for the modes at the Γ-point, and the results are shown in Figure 3; the agreement is excellent.

The librational modes about the *a* and *b* axes are calculated at 287 and 289 cm^{-1} and are somewhat higher than the observed value of 172 cm^{-1}. A series of calculations where the *a*/*c* lattice parameter ratio was varied by a few percent resulted in a shift of the librational modes but did not greatly change their energy. The difficulty of calculating the librational modes has been noted previously for $[NH_4]F$,[33]

(33) Adams, M. A.; Refson, K.; Gabrys, B. J. *Phys. Chem. Chem. Phys.* **2005**, *7*, 3685.

Table 2. Observed Bands (cm^{-1}) and Assignments for $Ba[ReH_9]$ in D_{3h} Symmetry

experimental (cm^{-1})			ab initio			assignment		
INS[a]	Raman	infrared	Γ-point (cm^{-1})	LOTO[b] (cm^{-1})	infrared intensity (km mol^{-1})	D_{6h}	D_3h	description
			0	0		E_{1u}	E'	*ab* acoustic mode
			0	0		A_{2u}	A_2'	*c* acoustic mode
			53	54		E_{2u}	E'	*a,b* Ba trans
49 w			57	55		E_{2g}	E'	*a,b* Re trans
			70	**70**	9.2	E_{1u}	E'	*b* Ba, Re trans
			70	**124**	9.2	E_{1u}	E'	*a* Ba, Re trans
78 w			87	88	15.9	A_{2u}	A_2''	*c* Re trans antiphase
			105	106		B_{1g}	A_2''	*c* Re trans in-phase
			126	126	5.3	B_{2u}	A_1'	*c* Ba trans
			152	157		B_{1u}	A_2'	*c* libration antiphase
136 s			162	167		A_{2g}	A_2'	*c* libration in-phase
			265	268	0.0	E_{1u}	E'	*c* prism squash antiphase
			266	270		E_{2g}	E'	*c* prism squash in-phase
172 s			287	288		E_{2u}	E'	*a,b* libration antiphase
256 vs			289	292		E_{1g}	E''	*a,b* libration in-phase
		684 s	683	**685**	0.9	E_{1u}	E'	ax−eq face breathing antiphase
680 m			683	**721**	0.9	E_{1u}	E'	
	711 br,w		698	700		E_{2g}	E'	ax−eq face breathing in-phase
730 s		740 sh	751	750	0.7	A_{2u}	A_2''	trigonal face out-of-phase symmetric bend antiphase
801			794	795		B_{1g}	A_2''	trigonal face out-of-phase symmetric bend in-phase
			821	821		E_{2u}	E''	ax−eq face rotation antiphase
860			823	824		E_{1g}	E''	ax−eq face rotation in-phase
			833	834		A_{1u}	A_1''	trigonal face out-of-phase torsion antiphase
			839	840		B_{2g}	A_1''	trigonal face out-of-phase torsion in-phase
			912	913		A_{2g}	A_1'	ax−eq out-of-phase rotation antiphase
			913	914		B_{1u}	A_2'	ax−eq out-of-phase rotation in-phase
			920	920		B_{2u}	A_1'	*c* ax symmetric deformation antiphase
920 s	925 m		921	922		A_{1g}	A_1'	*c* ax symmetric deformation in-phase
			939	938	0.1	A_{2u}	A_2''	*c* eq symmetric deformation antiphase
			941	941		B_{1g}	A_2''	*c* eq symmetric deformation in-phase
			990	991	0.0	E_{1u}	E'	ax−eq out-of-phase bend antiphase
991 s	983 m		992	993		E_{2g}	E'	ax-eq out-of-phase bend in-phase
			1068	1068		E_{2u}	E''	*c* eq bend in-phase
	1034 m		1068	1068		E_{1g}	E''	*c* eq bend antiphase
1053 s			1068	1068		E_{1g}	E''	*c* eq bend in-phase
		1830 sh	1836	1836	2.5	A_{2u}	A_2''	*c* ax trigonal face out-of-phase stretch in-phase
			1854	**1855**	1.6	E_{1u}	E'	symmetric prism edge stretch antiphase
		1870 s	1854	**1878**	1.4	E_{1u}	E'	
			1878	1879		B_{1g}	A_2''	*c* ax trigonal face out-of-phase stretch antiphase
			1879	1880		E_{2g}	E'	ax asymmetric stretch, trigonal faces in-phase
			1908	1908		E_{2u}	E''	ax asymmetric stretch, trigonal faces out-of-phase
1913			1927	1928		E_{1g}	E'	asymmetric prism edge stretch
			1966	1967		B_{2u}	A_1'	symmetric stretch ax and eq out-of-phase
			1969	1969		A_{1g}	A_2'	symmetric stretch ax and eq out-of-phase
		1956 sh	2038	**2039**	0.7	E_{1u}	E'	asymmetric eq stretch
1977			2038	**2052**	1.0	E_{1u}	E'	
			2043	2044		E_{2g}	E'	asymmetric eq stretch
			2072	2072		B_{2u}	A_1'	ax eq in-phase symmetric breathing
	1992 s		2077	2077		A_{1g}	A_1'	ax eq in-phase symmetric breathing

[a] s = strong, m = medium, w = weak, br = broad, v = very. [b] Modes significantly altered by inclusion of LOTO splitting are shown in bold.

where it was ascribed to anharmonicity in the librational mode. We believe that a similar situation appears to be the case here; unfortunately, the overtones of the librational modes are too weak to be distinguished, so we cannot prove the assertion beyond doubt. This highlights the need for further development of DFT-based lattice dynamics to include anharmonic corrections.

Table 2 lists the observed and calculated wavenumbers for the modes and gives an approximate description for the isolated ion. In the crystal, factor-group splitting results in each mode giving rise to an in-phase (*g*) and an out-of-phase (*u*) mode at the Γ-point. It can be seen that, in most cases, the splitting is 10 cm^{-1} or less. The splitting vanishes at the *A*-point because the ions move in the same direction.[34]

The dispersion curves are shown in Figures 4−6. Both the acoustic and optic translational modes show significant dispersion, 50−80 cm^{-1}. The calculations show that the librational modes are virtually dispersionless. The INS spectra are sensitive to modes across the entire Brillouin zone; thus for a crystalline material, the width of the peak reflects the dispersion. The modest width of the librational modes at 136 and 172 cm^{-1} supports the calculations.

The bending mode at 256 cm^{-1} and those in the 800−1100 cm^{-1} are almost dispersionless. The shape of the 920 cm^{-1} results from the overlap of two modes, rather than dispersion. This is not the case for the complex feature at

(34) Decius, J. C.; Hexter, R. M. *Molecular Vibrations in Crystals*; McGraw-Hill: New York, 1977.

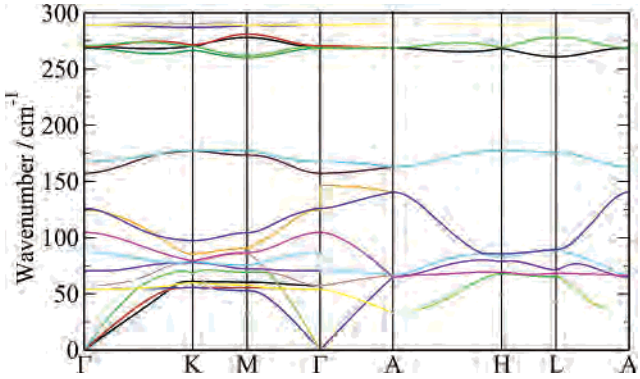

Figure 4. Dispersion curves of $Ba[ReH_9]$ for the 0−300 cm^{-1} region (lattice modes and the lowest internal modes).

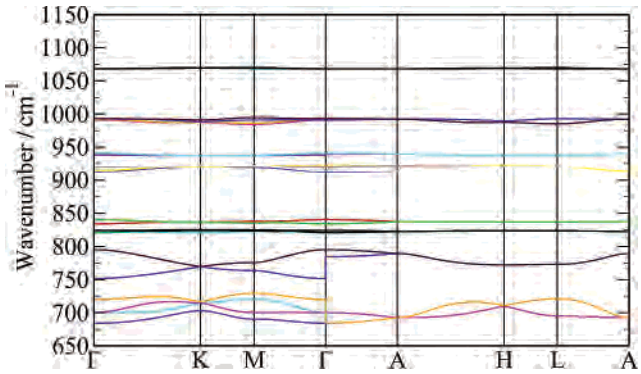

Figure 5. Dispersion curves of $Ba[ReH_9]$ for the 650−1150 cm^{-1} region (H−Re−H bending modes).

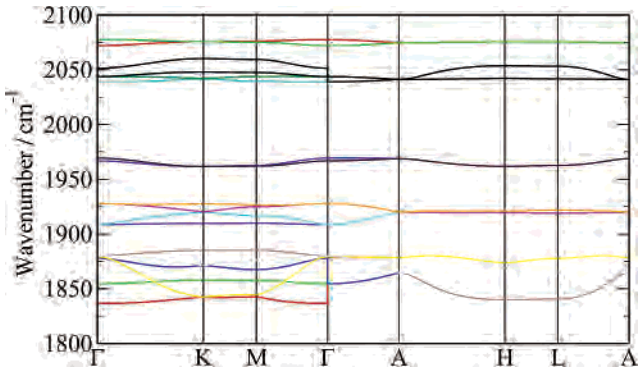

Figure 6. Dispersion curves of $Ba[ReH_9]$ for the 1800−2100 cm^{-1} region (Re−H stretching modes).

720 cm^{-1}: its shape results from the overlap of five modes, each of which exhibits ∼20 cm^{-1} dispersion. As is usually found, the stretching modes are largely undispersed.

Bonding. At first sight, it is surprising that the isolated ion calculations do so poorly in predicting the vibrational spectrum of the crystal. There is little shift of the frequencies between the solid and aqueous solution,[13] which might be regarded as being better modeled by isolated ions than the crystal. Conventional reasoning, based on nearest-neighbor Hamiltonian models, relates the ion-to-crystal frequency shift to the magnitude of the dispersion of the phonon branches. This predicts a splitting of molecular levels of a magnitude given by the intermolecular term and that the size dispersion gives an upper bound to the shift of molecular levels in a solid-state environment. That is clearly not the case in Ba-

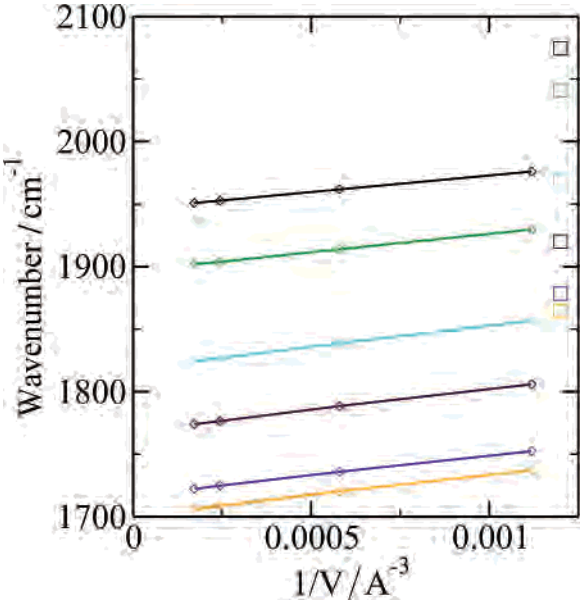

Figure 7. Frequencies of a single $[ReH_9]^{2-}$ ion calculated in periodic supercell using CASTEP as a function of cell volume (i.e., distance between $[ReH_9]^{2-}$ ions) for the six highest molecular modes. Also plotted are the *A*-point (where there is no factor-group splitting) frequencies of the solid (equivalent volume of 0.0044 $Å^{-3}$).

Table 3. Atomic Orbital Populations, Mulliken Charges and Born Effective Charges for $Ba[ReH_9]$

species	s	p	d	total	Mulliken charge	Born effective charges
H_{cap}	1.20			1.20	−0.20	$xx = -0.647$ $yy = 0.260$ $zz = 0.156$
H_{prism}	1.21			1.21	−0.21	$xx = -0.736$ $yy = 0.122$ $zz = 0.230$
Re	0.33	0.19	6.01	6.53	+0.47	$xx = -1.769$ $yy = -1.772$ $zz = -1.757$
Ba	2.03	6.00	0.60	8.63	+1.37	$xx = 2.668$ $yy = 2.668$ $zz = 3.037$

$[ReH_9]$, where most of the internal modes are dispersed by 20 cm^{-1} or less and a maximum of 50 cm^{-1}.

Using the periodic boundary condition code CASTEP, we were able to calculate the frequencies of an isolated $[ReH_9]^{2-}$ ion at exactly the same level of approximation as the full-crystal lattice dynamics. In this case, the physical model is an interacting periodic array of ions with a homogeneous positive charge to ensure electroneutrality. The non-interacting ion result is recovered in the infinite-cell size limit. The result is plotted in Figure 7 for the six highest molecular modes along with the corresponding crystalline modes at the *A* point. In contrast to the symmetrical splitting behavior of the dispersion along Γ−*A*, the crystal modes are all upshifted by 130−160 cm^{-1} compared to the isolated ion. An extrapolation of the ion frequencies to the reciprocal crystal volume (0.004 $Å^{-3}$) predicts upshifts of 100−150 cm^{-1}, entirely on the basis of the long-range limiting behavior of the intermolecular interaction. The failure of the simple model of molecular-level splitting may be understood by noting that the interionic interactions have a Coulombic component. The long-ranged nature of this means that the

Table 4. Shared Electron Numbers for $Ba[ReH_9]$

	$Re-H_{cap}$	$Re-H_{prism}$	$H_{cap}-H_{cap}$	$H_{prism}-H_{prism}$	$H_{cap}-H_{prism}$	$Ba-H_{cap}$	$Ba-H_{prism}$
shared electrons (electron)	0.37	0.48	−0.03	0.00	0.03	0.01	0.05
distance (Å)	1.668	1.705	2.346	2.100	1.915	2.763	2.899

splitting is not approximated by nearest-neighbor interactions but that infinite lattice sums are required to sum the contributions from distant periodic replicas. The extrapolation of the modes to the crystal cell volume demonstrates that this Coulombic interaction is the dominant part of the interaction in this case.

Projection of the plane waves onto an atomic basis set allows the atomic populations and Mulliken charges to be determined. Born effective charges (sometimes known as dynamical charges) are calculated using the density functional perturbation theory electric field response. The results are shown in Table 3. It can be seen that the hydrogens have a hydridic character (charge of −0.2) and that the cap and prism hydrogens are essentially identical. The rhenium carries a small positive charge of +0.47 in contrast to its formal charge of +7. The 5d-orbital occupancy of 6 electrons is higher than that for the neutral-atom configuration, indicating that these are the orbitals mainly involved in the bonding. The barium ion is closest to its formal charge of +2, while the electrons are largely lost from the 6s orbital as expected (the 2.03 electron occupancy for s orbitals in Table 3 is a sum over the 5s and 6s orbitals); it is surprising that there is some occupancy of the 5d-orbitals. The Born effective charges give a more complex picture. As is common, the magnitudes are larger than the Mulliken static charges, and for rhenium, the sign is opposite. The large magnitudes will give rise to significant polarization during vibration, which accounts for the substantial long-range interaction observed. A large anisotropy in the charge tensors is apparent for H, but the traces are close to the Mulliken values. The anisotropy is indicative of directional covalent bonding to the Re atom, and the negative overall dynamical charge confirms the hydridic nature of the protons.

The occupancy of the barium 5d-orbitals would indicate some degree of covalency between the barium and the hydrogen as does the nonzero shared-electron counts. There is also a clear distinction between the cap and prism hydrides. These features are also seen in the shared electron numbers for $Ba[ReH_9]$, Table 4. This shows that there is essentially zero interaction between the hydrides, confirming the assignment as a polyhydride. However, there is a small interaction between the barium ion and the nearest prism hydrides. These are somewhat more electron rich than the cap hydrides, perhaps accounting for the interaction.

Conclusions

In the present work, we have recorded the complete vibrational spectrum of the $[ReH_9]^{2-}$ ion. For both the infrared and INS spectra, we have used the comparison between the observed and calculated spectra to validate our ab initio periodic DFT results. This has also provided the first complete assignment of all of the modes of the ion. Analysis of the electronic structure shows that the bonding between the rhenium and the hydrogen is largely covalent. There is also a small degree of covalency between the prism hydrides and the barium.

This is typical of the picture that has emerged from the study of the ternary transition metal hydrides.[7,8] The alkali metal or alkaline earth counterion is crucial to the stability of the materials. As such, variation the counterion potentially offers a method to fine-tune the properties of the material.

The failure of the isolated ion methods is shown to be a consequence of the long-range Coulomb forces present and highlights the need for periodic DFT calculations to be able to understand these apparently simple systems.

Acknowledgment. The Rutherford Appleton Laboratory is thanked for access to neutron beam facilities. Computing resources (time on the SCARF computer used to perform the CASTEP calculations) was provided by CCLRC's e-Science facility. Manfred Bortz is thanked for assistance with the sample preparation.

IC0611894